



INVITED PAPER

A Tail's Tale: Biomechanical Roles of Dorsal Thoracic Spine of Barnacle Nauplii

Emily N. Branam,^{2,*} Jin Yung Wong,^{2,†,‡} Benny K. K. Chan,[†] Kit Yu Karen Chan ^{1*}

*Department of Biology, Swarthmore College, Swarthmore, PA 19081, USA; [†]Biodiversity Research Center, Academia Sinica, Taipei 11529, Taiwan; [‡]Department of Life Science, National Taiwan Normal University, Taipei 11677, Taiwan

²Co-first authors

¹E-mail: kchan1@swarthmore.edu

Synopsis Many marine invertebrates have complex life histories that begin with a planktonic larval stage. Similar to other plankton, these larval invertebrates often possess protruding body extensions, but their function beyond predator deterrence is not well-documented. For example, the planktonic nauplii of crustaceans have spines. Using the epibiotic pedunculate barnacle *Octolasmis spp.*, we investigated how the dorsal thoracic spine affects swimming and fluid disturbance by comparing nauplii with their spines partially removed against those with intact spines. Our motion analysis showed that amputated *Octolasmis spp.* swam slower, in jerkier trajectories, and were less efficient per stroke cycle than those with intact spines. Amputees showed alterations in limb beat pattern: larger beat amplitude, increased phase lag, and reduced contralateral symmetry. These changes might partially help increase propulsive force generation and streamline the flow, but were insufficient to restore full function. Particle image velocimetry further showed that amputees had a larger relative area of influence, implying elevated risk by rheotactic predator. Body extensions and their interactions with limb motion play important biomechanical roles in shaping larval performance, which likely influences the evolution of form.

Introduction

Many marine plankton possess body extensions such as spines, horns, or setae (Martin et al. 2014). Various configurations of spines and other extensions in plankton can contribute toward form resistance to reduce sinking (Walsby and Xypolyta 1977; Padisák et al. 2003). The size increase associated with spines can also help deter size-limited predation (Schlüter et al. 1987; Padisák et al. 2003; Herzog et al. 2016). Operating in low to intermediate Reynold's number (Re), body extensions could have other biomechanical implications by changing drag force on the organisms' bodies (Koehl 1996, 1998; Wong et al. 2020a). Amputation experiments remain a useful method for understanding the biomechanical roles of various structures (Delcomyn 1991; Zhang et al. 2015). Focusing on the naupliar form, a common zooplankton body plan, we examined the biomechanical role of body extensions through spine removal.

Crustacean larvae make up a large proportion of planktonic biomass and play important roles as grazers and prey for higher trophic levels (Jefferson et al. 2001; Vargas et al. 2006; Chew et al. 2012). Despite the high diversity of crustaceans, the naupliar larval form remains conserved—a form that possesses three sets of jointed swimming appendages, namely the antennules, antennae, and mandibles (Williams 1994b; Dahms 2000; Martin et al. 2014). Furthermore, most nauplii have some other type of rigid body extension, for example, the caudal spine in copepods or frontal horns and the dorsal thoracic spine in barnacles (Martin et al. 2014). Understanding how these morphological features impact ecological functions could shed light on the evolution of this widespread form.

With typical sizes ranging from approximately 100 to 1000 μm and swimming speeds of 0.1–10 mm s^{-1} , most nauplii operate in low to intermediate Re where viscous forces dominate (Purcell 1977; Wong

Advance Access publication 27 April 2021

© The Author(s) 2021. Published by Oxford University Press on behalf of the Society for Integrative and Comparative Biology. All rights reserved. For permissions please email: journals.permissions@oup.com.

et al. 2018). Due to the laminar nature of low *Re* environments, reciprocal motion does not lead to net displacement (Purcell 1977). The tail to head metachronal wave pattern displayed by multi-legged crustaceans is deemed as the “biomechanically optimal stroke pattern” for achieving forward net displacement (Murphy et al. 2011; Zhang et al. 2014; Takagi 2015; Hayashi and Takagi 2020). Another way to break reciprocal motion is to change the effective area for propulsion between strokes, which can be achieved by fanning out the setae on the tips of their appendages during the power stroke (PS) and collapsing them into bundles during the recovery stroke (Koehl 1998; Lamont and Emler 2018; von Dassow and Emler 2020). Non-collapsible body extensions, such as spines and horns, can also affect the overall cross-sectional area of an individual, and thus, affect the amount of drag experienced.

In addition to nonmobile morphological features, for example, setae and spines, limb kinematics also influence swimming performance. For example, krill achieve higher swimming speeds by increasing their pleopod beat frequency (Swadlow et al. 2005). Increases in stroke amplitudes also increase net forward displacement (Murphy et al. 2011; Lenz et al. 2015). Given that krill have multiple pairs of limbs, limb coordination can lead to different swimming behaviors, such as hovering and fast forward motion (Ford and Santhanakrishnan 2020). For individuals with limbs that can be moved radially, body rotation can be instigated by limb pronation or supination as well as breaking contralateral (left–right) limb beat symmetry (Niimoto et al. 2020). Furthermore, many crustaceans, such as mysids, krill, and branchiopod nauplii, possess nonrigid appendages that can be flexed during the recovery stroke to minimize drag (Hessler 1985; Johnson and Tarling 2008). The flexible nature and the optimal bending range of appendages for propulsion is highly conserved across taxa from small plankton to large mammals (Lucas et al. 2014). Despite the ubiquity of body extensions among zooplankton, the ways in which they influence limb kinematics and the implications of their interactions for swimming are largely unknown.

Aside from whole-body displacement, limb kinematic differences also impact how fluid flows around the organism’s body (Jiang et al. 2002a, 2002b). This fluid flow is crucial for delivering food particle laden water to feeding areas and can emit signals to rheotactic predators (Kjørboe et al. 2010; Jiang and Kjørboe 2011). Body extensions such as horns and spines can increase the effective cross-sectional area of the organisms and/or act as tethers to further

direct flow for suspension feeding (Emler et al. 1985; Vogel 1988; Wong et al. 2020a). Recent comparison between feeding and nonfeeding barnacle nauplii suggests that loss of feeding favors morphological change as well as limb kinematics that favor more efficient and stealthier swimming (Wong et al. 2020a). Taking into account the biomechanical roles of body extensions on key ecological functions, such as feeding and predator avoidance, could help us better understand the diversification of naupliar form.

Despite being strongly conserved as a general form across crustaceans, the nauplius exhibits many variations in the details of its morphologies, making them a useful case study for analyzing the role of body extensions (Martin et al. 2014; Wong et al. 2018). Barnacles in the family Lepadidae and Poecilasmidae have very long dorsal thoracic spines and frontal horns when compared with other sessilian families (Wong et al. 2018). Here, we use *Octolasmis*, a genus of epibiotic barnacle living on the gills of decapods that exists at a morphological extreme, possessing a narrow head shield and long body extensions, to determine the role of the dorsal thoracic spine in locomotion. To quantify the potential effects of dorsal thoracic spines on swimming and fluid disturbance, we used video motion analysis, limb tracking, and particle image velocimetry to compare the kinematics and hydrodynamics of freely swimming nauplii with their dorsal thoracic spine intact and 50% of the dorsal thoracic spine surgically removed.

Materials and methods

Adult collection and larval culturing

The crab *Portunus sanguinolentus* was procured from a wet market in Keelung City, Taiwan. Adult *Octolasmis cor* were cut from the gills and the epibiotic *Octolasmis warwickii* were excised from the carapace. The adult barnacles were kept in 0.45 μm filtered seawater (FSW) and fed with newly hatched *Artemia* sp. *ad libitum* until the release of larvae. The newly released stage I nauplii were transferred to FSW at 34 psu and kept at room temperature ($\sim 25^\circ\text{C}$). Stage II individuals were randomly divided into control and cut treatment groups, hereafter amputees (Fig. 1). Half of the dorsal thoracic spine of the amputees was removed lengthwise with custom-made ultra-fine needles and micro-scalpels from tungsten wire and glass pipette, respectively, with the methods in Wong (2020). These individuals were observed with two distinct motion analysis setups at an individual—(field of view $\sim 2 \times 2$ mm for

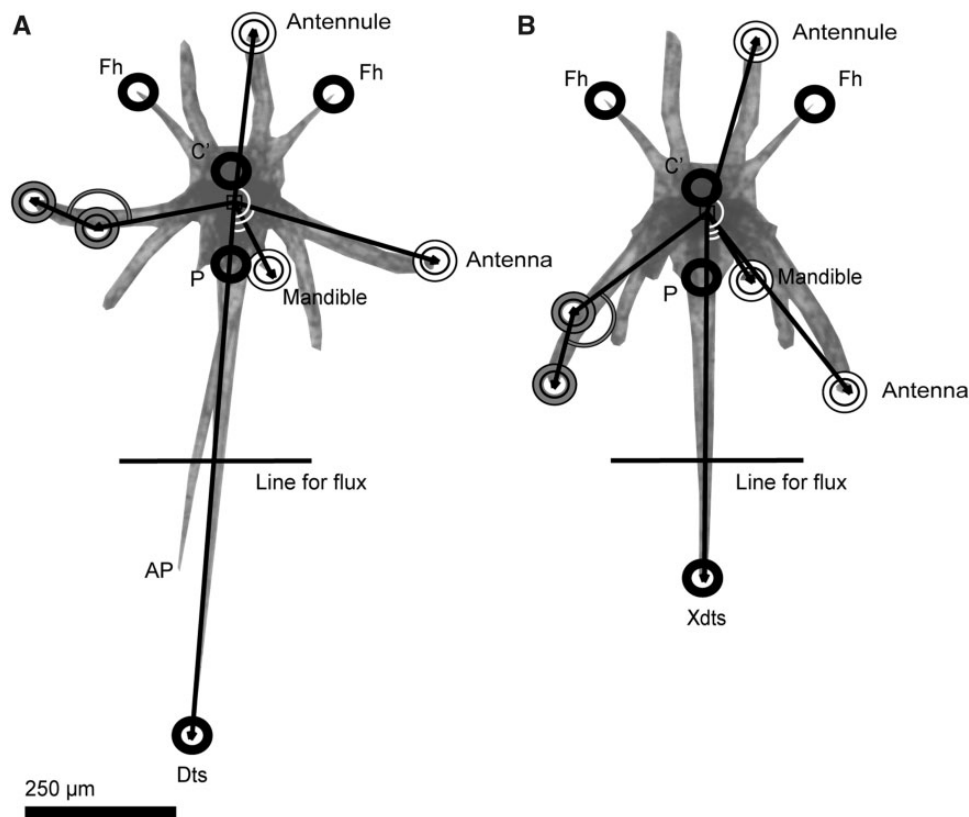


Fig. 1 Nauplii in the two treatment groups: (A) control and (B) amputated, showing landmarks used for kinematics analysis; Fh, frontal horn; Dts, dorsal thoracic spine; XDts, amputated dorsal thoracic spine; P, posterior point on head shield; C', head shield centroid. AP indicates the location of the abdominal process. Black lines indicate vectors from body centroid to appendage tips (CA) and body centroid to tip of dorsal thoracic spine (CP) for calculating limb angle, and vectors from centroid to point of maximum antenna curvature and curvature point to antenna tip for calculating flexion angle and ratio. Line for flux calculation is $3C'P$ from C'.

O. warwickii) and at a population scale (field of view 30×30 mm for *O. cor*).

Population scale observations on free swimming nauplii

Stage II *O. cor* nauplii were placed within 25 mL cell culture flasks immersed in a $25 \times 25 \times 25$ cm recirculating water bath kept at a temperature of 25°C . Larvae were kept in 34 psu FSW, illuminated by 850-nm infrared light, and filmed at 20 fps with an industrial GigE camera (GS132, Vezutech, Ltd., China) fitted with a 35–80 mm zoom lens at a resolution of 1280×1024 pixels. Swimming behavior of the nauplii was recorded for 6–7 min. New nauplii were used for each of the 4 replicates for each treatment. Edges of tanks were masked, and backgrounds were subtracted from each video with FOSICA (Wallingford Imaging Ltd.). Subsequent analysis was performed with the in-house Matlab program Tracker3D. Smoothing splines were applied to the resulting trajectories to remove frame rate noise and to detect overall direction of travel. For each path, the following metrics were computed: (1)

path duration; (2) gross speed (the first derivative of the smoothing spline); (3) net speed (the straight-line distance between start and end of a path divided by path duration); (4) net horizontal velocity ($U_{\text{free swim}}$); (5) net vertical velocity ($V_{\text{free swim}}$); (6) number of crossings across a mid-line approximating smoothing spline; (7) and average crossing distance. “Crossings” were defined as points where an individual path crossed its respective mid-line approximating smoothing spline (Fig. 2).

Individual scale observations on free swimming nauplii

The setup of high-speed video followed Chan et al. (2013) and Gemmell et al. (2014). *Octolasmis warwickii* nauplii were recorded in a $25 \times 75 \times 5$ mm glass cuvette with a FastCam Mini UX100 (Photron Ltd.) fitted with a bellows and a 60-mm focal length lens at $2000 \text{ frames s}^{-1}$ at 1280×1024 pixels (Wong et al. 2020a). Larvae were placed in a dark room and kept at 25°C using a larger buffer tank (400 mL). To trace fluid flow, the cuvettes were seeded with *Isochrysis galbana* (T-iso). Thirty individuals were

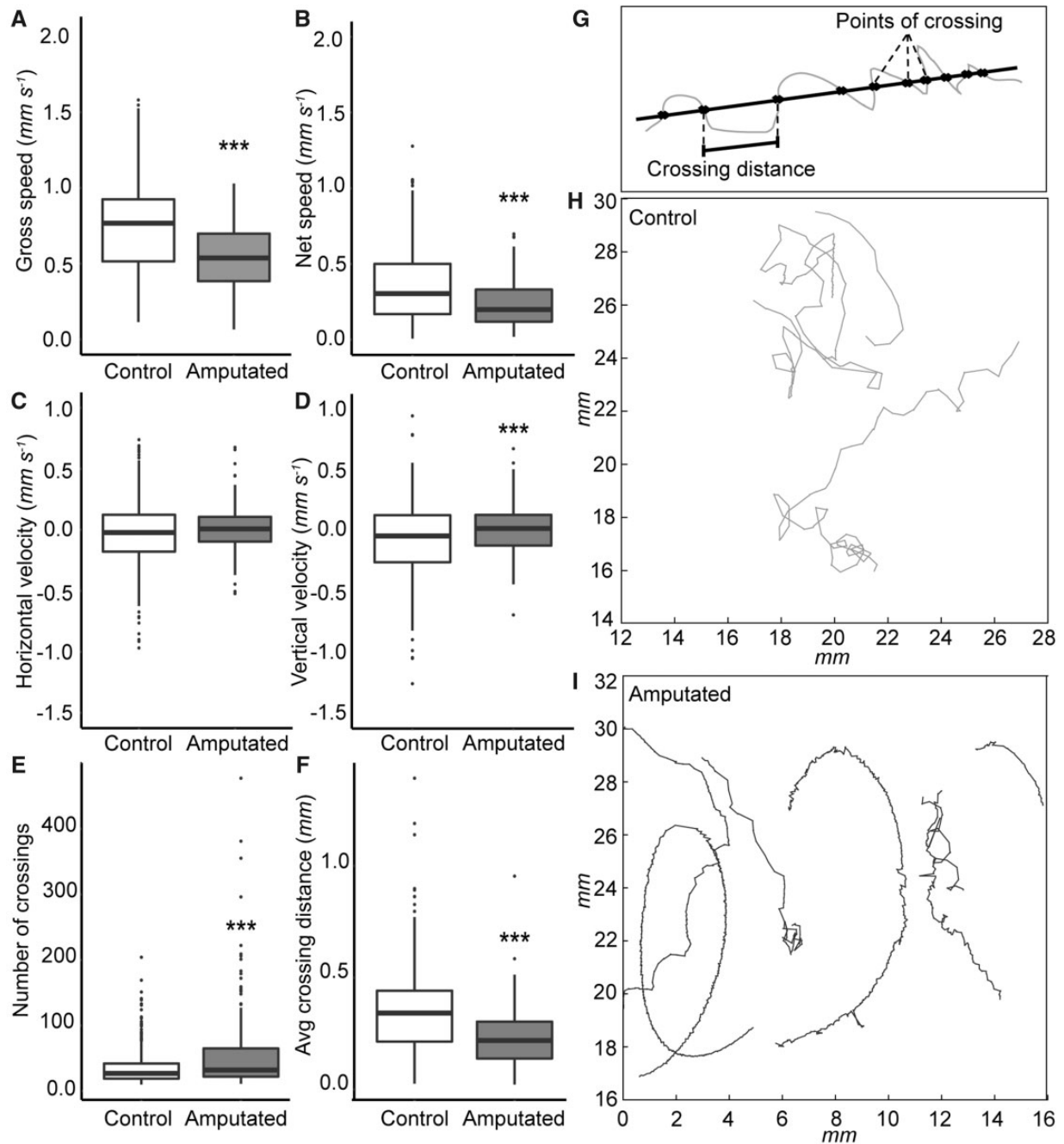


Fig. 2 Population-level observation of freely swimming *O. cor* nauplii. ((A–F) 267 and 170 trajectories for control and amputees, respectively). All boxplots compare control treatment (white) with amputated treatment (gray). Each box represents the first and third quartiles with maximum and minimum values represented by extended lines perpendicular to the box. Mean value is represented by the line within each box. *** $P < 0.001$. Swimming trajectory in gray and smoothing spline along the midline in black and “crossings” are marked with black crosses (G). Representative example swimming trajectories of control (H) and amputated nauplii (I).

used in each video session. All analyzed videos were taken from the dorsal/ventral view (xy plane).

Larval limb tracking

Larval limb positions were tracked across a complete stroke cycle for each individual at every 20th frame. The beginning of the PS was the time point in which the antennae were in their most rostrally extended

positions. The appendages on both the left and right side of the nauplii were tracked. The tip of each appendage (antennule, antennae, and mandible) was defined as the point at which the appendage ended and the setae began. Landmarking was performed with tpsDIG2 (version 2.31). To track the positioning of limbs in relation to the body, a body centroid was calculated from three body

landmarks—the tip of the left horn, right horn, and dorsal thoracic spine. For amputees, the third body landmark was placed at the point at which the spine was cut, reflecting the potential shift in center of mass (Fig. 1). Larvae displaying morphological abnormalities (bent tail or horns) were excluded from the limb kinematic analysis; 10 amputated nauplii videos and 9 control nauplii were compared.

The limb beat angle θ of a given appendage was the angle between the vector \overline{CA} (centroid to appendage tip) and \overline{CT} (centroid to dorsal thoracic spine tip). Angular separation between limb pairs on the left or right side of the body was calculated as a proxy for phase lag at four time points: start of PS, mid-PS, end of PS/start of recovery stroke, and mid recovery stroke. These time points were determined based on the limb beat angles of the right antennae because this pair of limbs was the major contributor to nauplii movement (Wong et al. 2020a). To test for contralateral symmetry in limb beats, we subtracted the limb beat angle of the right from the left. Whole larval movement was quantified with net displacement normalized with body length and forward to backward displacement ratio. Limb beat frequency was calculated based on the stroke duration.

Additionally, we tracked the flexion point and flexion ratio of the antennae across stroke cycle after Lucas et al. (2014). The flexion point was defined as the point of maximum curvature (Fig. 1). In instances of straight extensions, the tip of the appendage was marked as the flexion point. The angle of flexion (φ) was calculated as the dot product of the vectors from the flexion point to the body centroid \overline{CI} and from the flexion point to antenna tip \overline{CP} . The inflection ratio was the \overline{CI} divided by the sum of \overline{CI} and \overline{CP} .

Flow field analysis

Particle image velocimetry analysis followed Wong et al. (2020a). Using the software DaVis (version 8.2.1, LaVision GmbH), we visualized flow fields of each nauplius. Nauplii were masked algorithmically (smoothing, sliding maximum, and sliding minimum subtractions), followed by thresholding. Cross correlation computation on instantaneous velocity vectors was achieved using a multi-pass algorithm with decreasing interrogation window size from 64×64 to 32×32 pixels with 50% overlaps. Vector post processing removed outlier vectors. Final velocity vectors V_{flow} were exported as 80×64 cell grids for spatial attenuation and flux calculations (each cell represents 16×16 pixels with (u, v) components

representing velocity in the (x, y) directions). Flow fields around five representative individuals from each treatment group were compared.

Spatial attenuation of the flow (n), a factor that can influence detection by predators, was computed after Kjørboe et al. (2014), where

$$\| V_{\text{flow}} \| \propto r^n$$

Binning of flow speed was performed with different thresholds U^* , and r (magnitude of the spatial extent of flow) was determined as the radius of the circle of area equivalent to the area encompassed by binned speed (U^*). A power law fitting was used to estimate n as the slope of the regression.

Our earlier work showed flow toward the feeding area occurred during the recovery stroke (Wong et al. 2020a); thus, we computed the volume of fluid passing through a line segment (l) when the backwards velocity was largest. Given that the body centroid shifted with the amputation but the location of feeding region (labrum) did not, for a more accurate comparison, we defined the center of the head shield (C') using the landmarks of the horns and the posterior end of the head shield (P) where the dorsal thoracic spine protrudes (Fig. 1). The flux line was placed perpendicular to the vector $\overline{C'P}$ and centered at three $\overline{C'P}$ away from C' . To obtain a 2D estimate of the flux, we defined the length of the flux line to be $2 \times \overline{C'P}$, which roughly corresponded to the length of the head shield. The approximation of flux, ϕ , was calculated by taking the sum of the magnitude of velocity vectors projected on normal direction and multiplying it by velocity vector length,

$$\phi_{x,y} = \sum (u, v) \cdot \hat{n}d$$

1. where \hat{n} represents the normal unit vector and the dot product provides the magnitude of velocity vector projected onto the normal direction. Relative flux accounting for the nauplii velocity was calculated.

Statistical analysis

All statistical analyses were performed in R (version 3.6.2). Because multiple videos of each treatment were used for replication in the population level observation, we first checked for significance of a video identity for the video motion analysis using a Linear Mixed Effect Model with treatment categorized as a fixed effect and video identity (replication) as a random effect. Once we confirmed that video identity did not significantly affect the metric of interest, we

removed that factor and compare swimming with a *t*-test. Normality and homogeneity of variance were checked with Q–Q plot and *F*-test, respectively. Given the small sample size of the kinematic and flow field observations, we tested for the effect of amputation on those metrics with permutation *F*-tests (1000 permutations).

Results

Behavior of population scale freely swimming larvae

Treatment had significant effects on five of the seven metrics: Gross speed ($t_{1, 435} = 7.56$, $P < 0.001$), net speed ($t_{1, 435} = 6.03$, $P < 0.001$), net $V_{\text{free swim}}$ ($t_{1, 435} = -2.89$, $P = 0.004$), number of crossings ($t_{1, 435} = -4.27$, $P < 0.001$), and average crossing distance ($t_{1, 435} = 7.23$, $P < 0.001$; Fig. 2). In the control group, *O. cor* nauplii had mean gross speed 37.4% higher (observed difference: 0.2 mm s^{-1}) and mean net speed 53.9% higher (0.13 mm s^{-1}) than the amputees. Net V was significantly lower in control *O. cor* by an average of -6.6% (0.08 mm s^{-1}). There were significantly fewer crossings, spaced farther away in control *O. cor*, suggesting less convoluted paths (37.9 crossings in control compared with 58.3 crossings in amputated; 0.355 mm crossing distance in control compared with 0.229 mm in amputated).

Individual swimming kinematics

T1 F3 A 26.2% decrease in normalized speed was observed in *O. warwickii* amputees when compared with controls (Fig. 3 and Table 1). Forward: backward displacement ratio was lower in amputees by 38.9%. Amputated nauplii also displayed a lowered limb beat frequency by 8.8% (Table 1). Both treatment groups operated in *Re* near unity (1.83 ± 0.45 and 0.74 ± 0.37 for control and amputee, respectively). Significant differences in angular separation between the two treatment groups were also found across all but one time point and limb pair. The exception was the start of the PS between the antennule and antenna for both the left and right sides (Supplementary Table S1). Regarding limb beat symmetry, the difference between left and right mandible beat angle of amputees was 81.6% greater than control nauplii during mid-PS (Fig. 3). Amputees beat their limbs at significantly greater amplitudes than controls for all appendages but the right-side antennule (Table 1). Additionally, amputees straightened both antennae at the end of the PS more than controls. The flexion angle of amputees' antennae at the end of the PS was $>50\%$ smaller than the control for both the left and the right (Table 1). The flexion ratio also differed between treatments across multiple

time points, with flexion occurring closer to the larval body among amputees (Supplementary Fig. S1; Table 1).

Particle image velocimetry

While the differences in spatial attenuation displayed statistical significance between the two treatments, they were of the same order of 1 ($F_{1,8} = 4.98$, $P = 0.005$; Fig. 4). The area of influence, that is, area with flow velocity greater than the 80th percentile of all recorded velocity, were on average not different between the control and amputee ($F_{1,8} = 0.432$, $P = 0.5$). However, when normalized by the square of body length, the amputees created approximately 3-fold larger fluid disturbance (Fig. 4; $F_{1,8} = 12.4$, $P < 0.001$) The average relative flux for the amputee when body backward velocity was largest was comparable with that of the control ($F_{1,8} = 1.35$, $P = 0.289$). However, the results were highly variable between individuals with the standard deviations of $0.49 \text{ mm}^2 \text{ s}^{-1}$ for the control compared with $1.30 \text{ mm}^2 \text{ s}^{-1}$ for the amputated group (Fig. 4).

Discussion

Many planktonic organisms, including highly mobile natatory forms, have long body extensions suggesting that functions beyond anti-predation are likely. Using stage II barnacle nauplii from the genus *Octolasmis* that possess an extremely long dorsal thoracic spine relative to their size and to other barnacles, we investigated the biomechanical role of this body structure. Our observations highlighted that body extensions enhanced swimming proficiency and reduced predation risk. When the body extension was experimentally reduced in length, possibly compensatory changes in limb kinematics were observed: increased stroke amplitude and limb–limb angular separation to generate larger propulsive force, as well as reduced flexion angle at the beginning of the recovery stroke for streamlining. However, these changes were not sufficient to compensate for the reduction in the spine. These observations highlight how the interactions between rigid morphological structures, for example, spines, and moving limbs, shape key ecological functions of multi-legged swimmers.

Spine damage compromises swimming

Freely swimming, amputated *O. cor* nauplii were observed to have lowered net and gross speeds and “jerkier” swimming trajectories with higher numbers of crossings along the mid-line that were more closely spaced (Fig. 2). The observed swimming

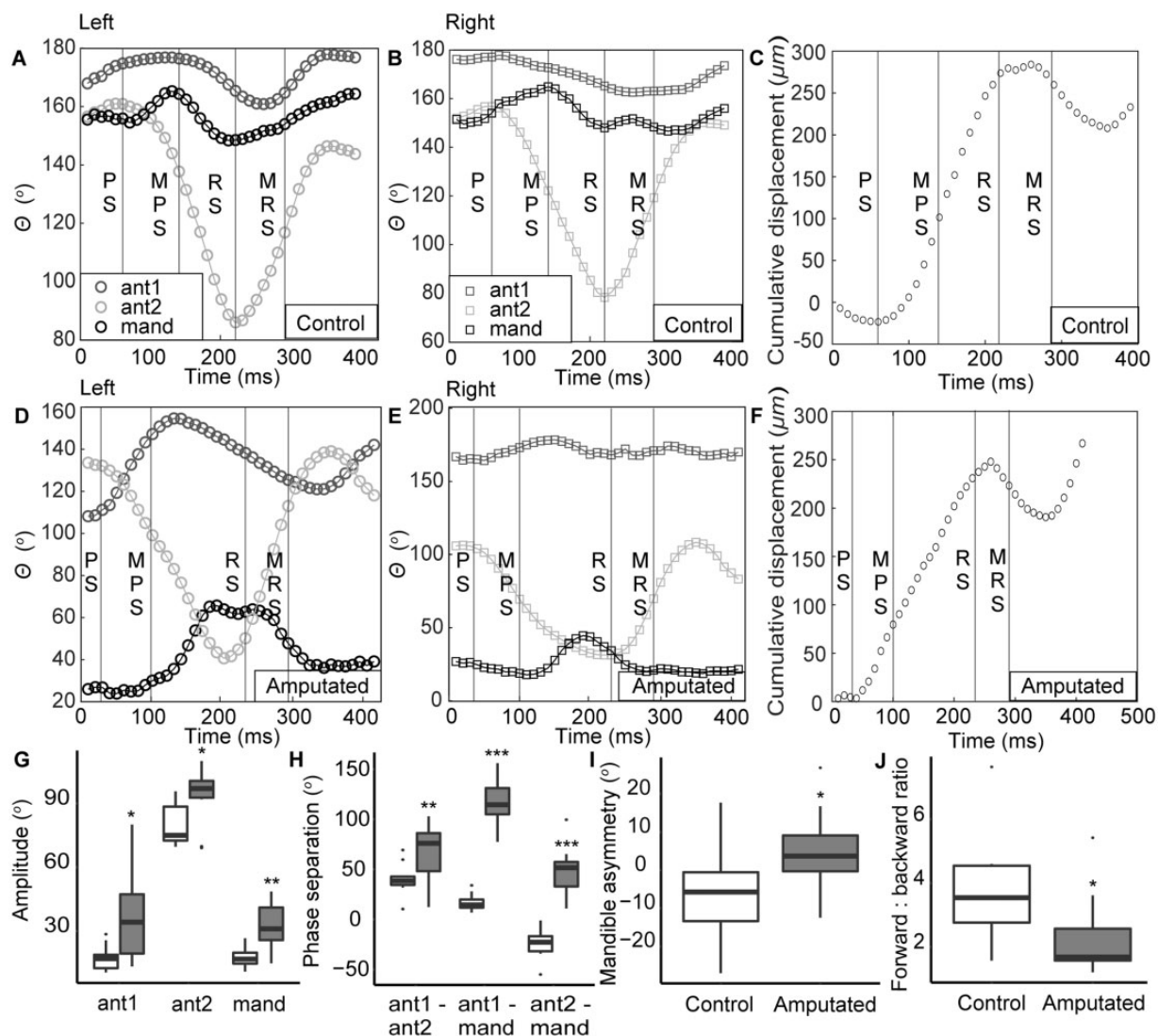


Fig. 3 Limb angle of control (A, B) and amputated (D, E) *O. warwickii* nauplii through one beat cycle. All 3 pairs of appendages (ant1, antennule; ant2, antenna; mand, mandible) on both the left and right were tracked. Vertical light gray lines denote the start of PS, mid-PS (MPS), start of recovery stroke (RS), and mid recovery stroke. Control larvae had higher net displacement (C, F) and forward:backward ratio than the amputees (J). Amputated nauplii had larger limb beat angle (G) and angular separation between limb pairs (H); only data on the left is shown. Largest difference in asymmetry between the left and the right pairs of limbs was recorded for the mandible during mid-PS (I). See Fig. 2 for the details of the boxplots. *, $P < 0.05$; **, $P < 0.01$; ***, $P < 0.001$.

speed reduction was reiterated among *O. warwickii* nauplii tracked with high-speed videography (Fig. 3). These observed differences between treatment groups were unlikely due to handling stress since both amputated and control nauplii were manipulated with a probe. Indeed, the change in swimming speed and overall trajectories were likely associated with the change in limb kinematics discussed below.

Loss of spine and reduction in swimming speed have functional implications, particularly for predator avoidance. The amputation could be interpreted as a proxy for injuries sustained during partial predation observed in nature (Ohman 1984; Elliott and Tang 2011). That spines assist in size deterrence is

well-documented among plankton (Schlüter et al. 1987; Herzog et al. 2016). Given that the *Octolasmis* nauplii we studied underwent a decrease in size of $>400 \mu\text{m}$ ($\sim 40\%$ of body length), an order of magnitude larger than the previously reported induced anti-predation responses, vulnerability to size-limited predators likely increased with spine length reduction. Some barnacle nauplii undertake diel vertical migrations, and a reduction of swimming speed could compromise the organisms' ability to keep speed with light attenuation rates (Richards et al. 1996; Bonicelli et al. 2016). Therefore, injuries incurred on body extensions could negatively affect survivorship.

Changes in limb kinematics

The observed reduction in swimming performance was accompanied by several changes in limb kinematics. First, amputees displayed higher limb beat amplitudes than controls. Numerical models of planktonic crustaceans suggested that increases in limb beat amplitude increase net displacement per stroke cycle until eventually plateauing due to limb interactions (Lenz et al. 2015; Takagi 2015). Second, the flexion angles of the antennae were smaller among amputated nauplii at the end of the PS, that is, straighter limbs, than controls. We focused on the antennae because they are generally the main propulsors in crustacean nauplii, and the mandibles are reduced and their activities harder to quantify (Gauld 1959; Moyse 1984; Williams 1994a). Swimming pteropods and the nauplii of other crustaceans at comparable Re are observed to orient their wings or limbs parallel to flow to minimize drag (Hessler 1985; Johnson and Tarling 2008). The observed reduction in flexion angle at the end of the PS might also contribute toward amputees' forward motion. It is important to note that in addition to streamlining, these flexible limbs were also effective thrust generating propulsors: the flexion angles at the beginning of the PS were 19.5° and 25.6° for control and amputated nauplii, matching the universal optimal range of maximum propulsor flexion angle (Lucas et al. 2014). These two kinematic adjustments (increased amplitude and decreased curvature) may act in conjunction to partially compensate for the loss of the spine. However, it is important to note that with a $Re \approx 1$, streamlining during recovery stroke translated into further backward displacement. As a result, the amputees were less efficient at swimming forward per stroke cycle.

A third change in limb kinematics was the increased phase lag between pairs of limbs when spines were amputated. Previous comparisons between planktotrophic and lecithotrophic barnacle nauplii suggested that anti-phase beating of the appendages provided additional anchoring effects and helped direct food particles toward the food capture area (Wong et al. 2020a). For *O. warwickii*, we observed that at the end of the recovery stroke, due to the larger angular separation, antenna and mandible moved in opposite directions, and on occasion, touched each other (Fig. 3 and Table 1). A large phase lag and the resulting limb–limb interactions were shown to reduce net displacement in copepods and krill (Lenz et al. 2015; Ford et al. 2019; Ford and Santhanakrishnan 2020). Perhaps, the increased phase lag observed helps dampen the backward

displacement during recovery stroke after spine removal.

The fourth and final change in kinematics were the shift in contralateral synchrony, that is, the asynchronous beating of the left and right pairs of appendages (Fig. 3 and Table 1). For copepod nauplii, yaw occurred as a result of pronation or supination of the antenna such that one side drove more fluid motion than the other (Niimoto et al. 2020). We observed a significant change in mandible symmetry during mid-PS in amputated nauplii, which likely translated into yaw. Partial removal of the dorsal thoracic spine not only reduced form drag, but also likely influenced weight distribution and stability, that is, the ability to maintain directed motion (Grünbaum and Strathmann 2003). The observed behaviors associated with body rotation could possibly be another form of (partial) compensation, and the mechanosensory feedback that underlies such behaviors warrants further investigation.

Change in velocity field

The observed differences in overall morphology and limb kinematics led to a shift in flow field around the nauplii such that amputees had a larger normalized area of influence (Fig. 4). The risk of predation by rheotactic predator is proportional to this fluid signal (Kjørboe et al. 2014). Hence, it is reasonable to predict that loss of spine increases predation risk, which agrees with the field observations that dead copepod nauplii are often partially consumed (Elliott and Tang 2011). The average spatial attenuation (n) of both groups was ~ 1 (Table 1), which was comparable with values observed for the planktonic nauplii of *Tetraclita japonica* and *Capitulum mitella* (Wong et al. 2020a, 2020b). Compared with an $n \approx 3$ for the lecithotrophic *Polyascus planus*, the extremely long dorsal thoracic spine of *Octolasmis* did not appear to aid in flow attenuation. Delivery of food laden water to the labrum, and thus, feeding efficiency is determined by the flux, that is, velocity of water per unit area. The measured relative flux toward the labrum remained comparable between amputee and the control. This lack of difference was likely due to the fact that relative flux toward the larval body was mostly attributed to body motion, which was an order of magnitude larger than the flow induced by the beating appendages (here and in Andersen and Kjørboe 2020; Wong et al. 2020a). However, the relative flux was more variable among amputated individuals, which could still imply reduction in time-integrated clearance. Vorticity and particle tracking velocimetry studies could

Table 1 Limb kinematics and fluid disturbance of control and amputated *O. warwickii* nauplii

	Control ($\bar{x} \pm \text{SD}$)	Amputated ($\bar{x} \pm \text{SD}$)	F	P-value
Speed (mm s^{-1})	1.65 ± 0.305	1.25 ± 0.359	6.52	0.028
Forward: backward displacement ratio	3.81 ± 1.72	2.33 ± 1.31	4.52	0.045
Beat frequency (Hz)	2.53 ± 0.128	2.31 ± 0.123	15.1	0.004
Asymmetry (°)				
Ant1				
PS:	0.879° ± 8.07°	−3.23° ± 25.6°	0.211	0.667
MPS:	1.37° ± 8.52°	−0.518° ± 19.8°	0.0694	0.822
RS: MRS:	1.34° ± 6.43°	−2.06° ± 16.5°	0.336	0.580
	2.78° ± 10.1°	−4.82° ± 13.9°	1.81	0.197
Ant2				
PS:	−1.31° ± 10.2°	−6.19° ± 17.7°	0.520	0.467
MPS:	0.900° ± 15.6°	−4.60° ± 26.0°	0.302	0.582
RS: MRS:	1.44° ± 11.0°	4.63° ± 16.6°	0.238	0.613
	−0.386° ± 6.43°	0.316° ± 25.4°	0.00670	0.939
Mand				
PS:	−4.17° ± 11.1°	0.582° ± 14.9°	0.615	0.448
MPS:	−6.56° ± 12.7°	5.36° ± 10.8°	4.87	0.035
RS: MRS:	−3.35° ± 5.34°	4.08° ± 11.5°	3.14	0.102
	−3.28° ± 10.4°	3.58° ± 8.37°	2.54	0.144
Amplitude (°)				
Left-ant1	17.6° ± 6.16	36.8° ± 20.9°	6.95	0.014
Left-ant2	80.5° ± 10.2°	93.5° ± 13.7°	5.46	0.037
Left-mand	17.5° ± 4.40°	31.6° ± 11.4°	12.2	0.002
Right-ant1	19.3° ± 5.54°	24.4° ± 13.7°	1.08	0.358
Right-ant2	80.6° ± 10.7°	95.3° ± 16.4°	5.25	0.045
Right-mand	19.5° ± 6.83°	29.6° ± 7.29°	9.62	0.008
Flexion angle (°)				
Left-ant2				
PS:	14.7° ± 11.6°	23.2° ± 11.5°	2.54	0.117
MPS:	31.6° ± 32.3°	48.2° ± 26.7°	1.50	0.225
RS: MRS:	108° ± 11.8°	51.0° ± 27.0°	34.3	0.001
	61.5° ± 42.7°	44.9° ± 26.7°	1.06	0.329
Right-ant2				
PS:	19.6° ± 14.4°	25.8° ± 9.26°	1.27	0.295
MPS:	48.9° ± 41.3°	49.0° ± 23.3°	0.00	0.996
RS: MRS:	105° ± 19.4°	47.2° ± 20.2°	40.5	0.001
	61.4° ± 36.0°	45.4° ± 23.6°	1.34	0.258
Flexion ratio				
Left-ant2				
PS:	0.837 ± 0.071	0.730 ± 0.114	5.88	0.019
MPS:	0.801 ± 0.087	0.739 ± 0.101	2.02	0.189
RS: MRS:	0.652 ± 0.047	0.691 ± 0.092	1.33	0.244
	0.764 ± 0.055	0.694 ± 0.079	4.95	0.048
Right-ant2				
PS:	0.835 ± 0.046	0.720 ± 0.059	22.2	<0.001

(continued)

Table 1 Continued

	Control ($\bar{x} \pm \text{SD}$)	Amputated ($\bar{x} \pm \text{SD}$)	<i>F</i>	<i>P</i> -value
MPS:	0.783 ± 0.062	0.739 ± 0.099	1.30	0.321
RS: MRS:	0.662 ± 0.057	0.639 ± 0.057	0.452	0.509
	0.792 ± 0.045	0.699 ± 0.083	8.91	0.008
Absolute area of influence (mm ²)	0.646 ± 0.032	0.663 ± 0.05	0.432	0.500
Body length ² normalized area of influence	0.621 ± 0.07	2.05 ± 0.90	4.98	0.005
Spatial attenuation power (<i>n</i>)	-1.17 ± 0.040	-1.28 ± 0.102	12.4	<0.001
Relative flux (mm ² s ⁻¹)	-1.39 ± 0.439	0.495 ± 1.49	1.35	0.289

MPS: mid-PS, RS: start of recovery stroke, MRS: mid-recovery stroke. Ant1: antennule, ant2: antennae, mand: mandible. Values of statistically significant differences ($P < 0.05$) are given in bold-face.

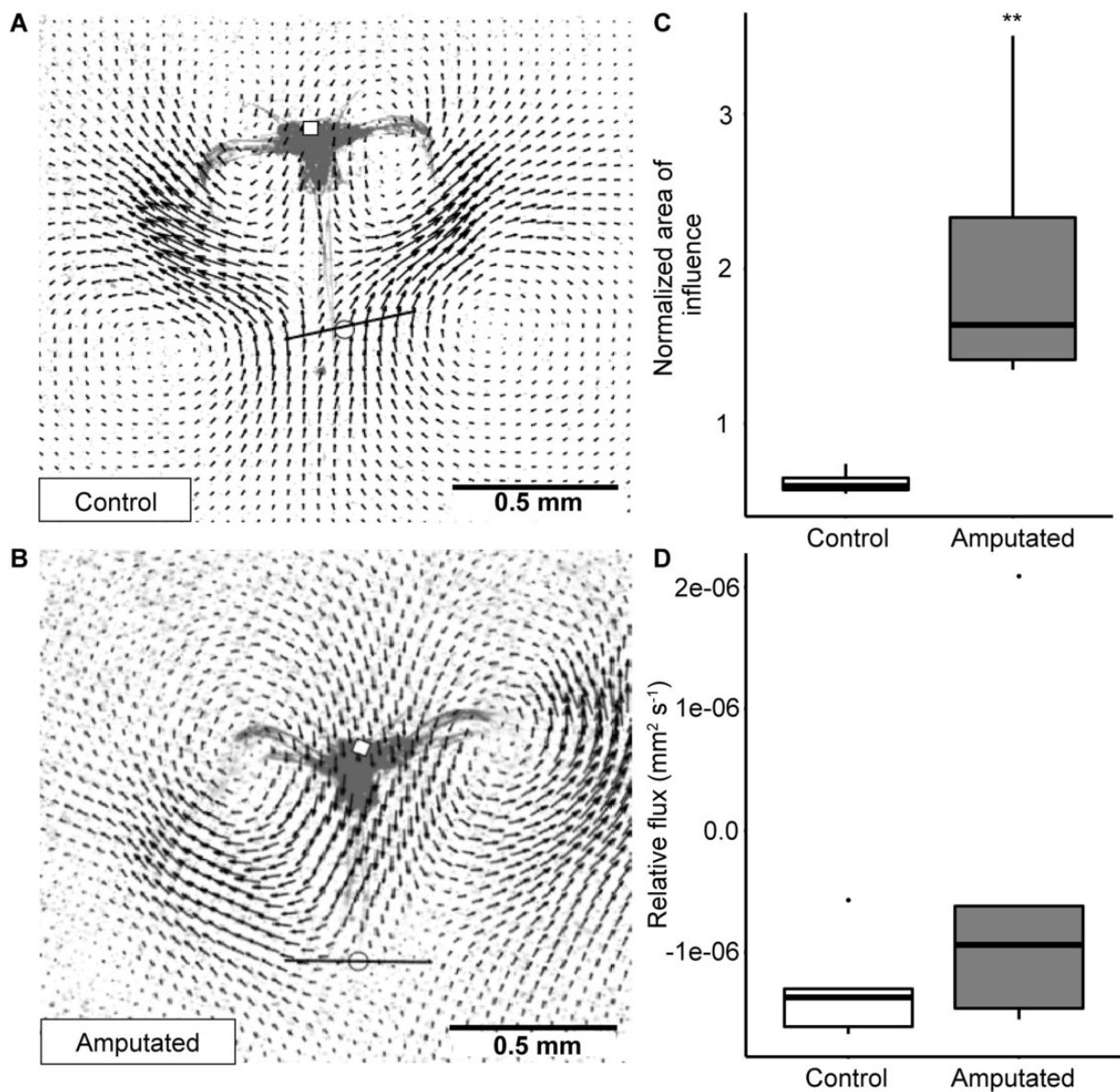


Fig. 4 Flow field around representative nauplii with spine intact (A) and amputated (B) at the moment of maximum body backward displacement in a stroke cycle. Open squares mark the head shield centroid, open circles mark the midpoint of the flux line (black). The area of influence was normalized by squared body-length and was found to be significantly higher for amputees (C), but the relative flux was comparable between the two groups after accounting for body velocity (D). ** $P < 0.01$.

confirm these two proposed reductions in ecological functions by detailing the viscous vortex ring structures and testing whether particles enter the labrum.

Body extensions of zooplankton are not only rigid structures for predator deterrence and buoyancy regulation. Our observations on barnacle nauplii with extremely long dorsal thoracic spine showed that these extensions also interact with the flexible beating appendages to affect swimming speed and the size-normalized flow disturbance around an individual. Nevertheless, this interaction could become more important through ontogeny as the dorsal thoracic spine lengthens and appendage setations become more complicated. For small plankton operating in low to intermediate Re , these changes in flow field in turn shape their abilities to capture food particles and avoid predation. The biomechanical and behavioral constraints associated with these limb–spine interactions likely influenced the evolution and diversification of crustacean naupliar form.

Funding

This work was supported by the Ministry of Science and Technology, Taiwan (106-2923-B-001-002-MY3; to B.C.); the Croucher Foundation and Faculty Research Fund from Swarthmore College (to K.C.); and the Taiwan International Graduate Program PhD Fellowship (to J.W.).

Data availability statement

The data underlying this article is available at <https://osf.io/sg5a8/>.

Acknowledgments

The authors thank D. Tong, E. Wong, H. Tso, Y. K. Tam, and P.C. Tsoi for technical support and W.H. Ko for analysis assistance.

References

- Andersen A, Kiørboe T. 2020. The effect of tethering on the clearance rate of suspension-feeding plankton. *Proc Natl Acad Sci U S A* 117:30101–3.
- Bonicelli J, Tyburczy J, Tapia FJ, Finke GR, Parragué M, Dudas S, Menge BA, Navarrete SA. 2016. Diel vertical migration and cross-shore distribution of barnacle and bivalve larvae in the central Chile inner-shelf. *J Exp Marine Biol Ecol* 485:35–46.
- Chan KYK, Jiang H, Padilla DK. 2013. Swimming speed of larval snail does not correlate with size and ciliary beat frequency. *PLoS One* 8:e82764.
- Chew LL, Chong VC, Tanaka K, Sasekumar A. 2012. Phytoplankton fuel the energy flow from zooplankton to small nekton in turbid mangrove waters. *Marine Ecol Progr Ser* 469:7–24.
- Dahms H-U. 2000. Phylogenetic implications of the crustacean nauplius. *Hydrobiologia* 417:91–9.
- Delcomyn F. 1991. Perturbation of the motor system in freely walking cockroaches. I. Rear leg amputation and the timing of motor activity in leg muscles. *J Exp Biol* 156:483–502.
- Elliott DT, Tang KW. 2011. Spatial and temporal distributions of live and dead copepods in the lower Chesapeake Bay (Virginia, USA). *Estuaries Coasts* 34:1039–48.
- Emler R, Strathman R, Strickler J. 1985. Gravity, drag, and feeding currents of small zooplankton. *Science* 228:1016–7.
- Ford M, Santhanakrishnan A. 2020. On the role of phase lag in multi-appendage metachronal swimming of euphausiids. *Bioinspir Biomimet* doi: 10.1088/1748-3190/abc930.
- Ford MP, Lai HK, Samaee M, Santhanakrishnan A. 2019. Hydrodynamics of metachronal paddling: effects of varying Reynolds number and phase lag. *Royal Soc Open Sci* 6:191387.
- Gauld D. 1959. Swimming and feeding in crustacean larvae: the nauplius larva. *Proc Zool Soc Lond* 132:31–50.
- Gemmell BJ, Jiang H, Buskey EJ. 2014. A new approach to micro-scale particle image velocimetry (μ PIV) for quantifying flows around free-swimming zooplankton. *J Plankton Res* 36:1396–401.
- Grünbaum D, Strathmann RR. 2003. Form, performance and trade-offs in swimming and stability of armed larvae. *J Marine Res* 61:659–91.
- Hayashi R, Takagi D. 2020. Metachronal swimming with rigid arms near boundaries. *Fluids* 5:24.
- Herzog Q, Tittgen C, Laforsch C. 2016. Predator-specific reversibility of morphological defenses in *Daphnia barbata*. *J Plankton Res* 38:771–80.
- Hessler RR. 1985. Swimming in Crustacea. *Earth Environ Sci Trans Royal Soc Edinburgh* 76:115–22.
- Jefferson TT, Henrik L, Torkel Gissel N, Benni Winding H. 2001. Zooplankton feeding ecology: grazing on phytoplankton and predation on protozoans by copepod and barnacle nauplii in Disko Bay, West Greenland. *Marine Ecol Progr Ser* 221:209–19.
- Jiang H, Kiørboe T. 2011. The fluid dynamics of swimming by jumping in copepods. *J Royal Soc Interf* 8:1090–103.
- Jiang H, Meneveau C, Osborn TR. 2002a. The flow field around a freely swimming copepod in steady motion. Part II: numerical simulation. *J Plankton Res* 24:191–213.
- Jiang H, Osborn TR, Meneveau C. 2002b. The flow field around a freely swimming copepod in steady motion. Part I: theoretical analysis. *J Plankton Res* 24:167–89.
- Johnson ML, Tarling GA. 2008. Influence of individual state on swimming capacity and behaviour of Antarctic krill *Euphausia superba*. *Marine Ecol Progr Ser* 366:99–110.
- Kiørboe T, Jiang H, Colin SP. 2010. Danger of zooplankton feeding: the fluid signal generated by ambush-feeding copepods. *Proc Royal Soc B: Biol Sci* 277:3229–37.
- Kiørboe T, Jiang H, Gonçalves RJ, Nielsen LT, Wadhwa N. 2014. Flow disturbances generated by feeding and swimming zooplankton. *Proc Natl Acad Sci U S A* 111:11738–43.
- Koehl M. 1998. Small-scale hydrodynamics of feeding appendages of marine animals. *Oceanography* 11:10–2.
- Koehl MAR. 1996. When does morphology matter? *Ann Rev Ecol Syst* 27:501–42.

- Lamont EI, Emler RB. 2018. Permanently fused setules create unusual folding fans used for swimming in cyprid larvae of barnacles. *Biol Bull* 235:185–94.
- Lenz PH, Takagi D, Hartline DK. 2015. Choreographed swimming of copepod nauplii. *J Royal Soc Interf* 12:20150776.
- Lucas KN, Johnson N, Beaulieu WT, Cathcart E, Tirrell G, Colin SP, Gemmell BJ, Dabiri JO, Costello JH. 2014. Bending rules for animal propulsion. *Nat commun* 5:7.
- Martin JW, Olesen J, Høeg JT, Høeg J. 2014. Atlas of crustacean larvae. Baltimore (MD): JHU Press.
- Moyle J. 1984. Some observations on the swimming and feeding of the nauplius larvae of *Lepas pectinata* (Cirripedia: crustacea). *Zool J Linnean Soc* 80:323–36.
- Murphy D, Webster D, Kawaguchi S, King R, Yen J. 2011. Metachronal swimming in Antarctic krill: gait kinematics and system design. *Marine Biol* 158:2541–54.
- Niimoto K, Kuball KJ, Block LN, Lenz PH, Takagi D. 2020. Rotational maneuvers of copepod nauplii at low Reynolds number. *Fluids* 5:78.
- Ohman MD. 1984. Omnivory by *Euphausia pacifica*: the role of copepod prey. *Marine ecology progress series*. Oldendorf 19:125–31.
- Padisák J, Soróczki-Pintér É, Rezner Z. 2003. Sinking properties of some phytoplankton shapes and the relation of form resistance to morphological diversity of plankton—an experimental study. *Hydrobiologia* 500:243–57.
- Purcell EM. 1977. Life at low Reynolds number. *Am J Phys* 45:3–11.
- Richards SA, Possingham HP, Noye J. 1996. Diel vertical migration: modelling light-mediated mechanisms. *J Plankton Res* 18:2199–222.
- Schlüter M, Groeneweg J, Soeder CJ. 1987. Impact of rotifer grazing on population dynamics of green microalgae in high-rate ponds. *Water Res* 21:1293–7.
- Swadlow K, Ritz D, Nicol S, Osborn J, Gurney L. 2005. Respiration rate and cost of swimming for Antarctic krill, *Euphausia superba*, in large groups in the laboratory. *Marine Biol* 146:1169–75.
- Takagi D. 2015. Swimming with stiff legs at low Reynolds number. *Phys Rev E* 92:023020.
- Vargas CA, Manríquez PH, Navarrete SA. 2006. Feeding by larvae of intertidal invertebrates: assessing their position in pelagic food webs. *Ecology* 87:444–57.
- Vogel S. 1988. *Life's Devices: the physical world of animals and plants*. Princeton University Press. Princeton, New Jersey, USA.
- von Dassow G, Emler RB. 2020. Direct observation of the setular web that fuses thoracopodal setae of a calanoid copepod into a collapsible fan. *Biol Bull* 238:73–9.
- Walsby A, Xypolyta A. 1977. The form resistance of chitan fibres attached to the cells of *Thalassiosira fluviatilis* Hustedt. *Br Phycol J* 12:215–23.
- Williams TA. 1994a. A model of rowing propulsion and the ontogeny of locomotion in *Artemia* larvae. *Biol Bull* 187:164–73.
- Williams TA. 1994b. The nauplius larva of crustaceans: functional diversity and the phylotypic stage. *Am Zool* 34:562–9.
- Wong JY. 2020. Comparative biomechanics of barnacle larvae. Taiwan: National Taiwan Normal University.
- Wong J, Chan KK, Chan BK. 2018. Phylogenetic, ecological and biomechanical constraints on larval form: a comparative morphological analysis of barnacle nauplii. *PLoS One* 13:e0206973.
- Wong J, Chan BK, Chan K. 2020a. Evolution of feeding shapes swimming kinematics of barnacle naupliar larvae: a comparison between trophic modes. *Integr Organism Biol* 2:obaa011.
- Wong J, Chan BK, Chan KK. 2020b. Swimming kinematics and hydrodynamics of barnacle larvae throughout development. *Proc Royal Soc B* 287:20201360.
- Zhang C, Guy RD, Mulloney B, Zhang Q, Lewis TJ. 2014. Neural mechanism of optimal limb coordination in crustacean swimming. *Proc Natl Acad Sci U S A* 111:13840–5.
- Zhang Y, Zhang J, Ren L. 2015. The terrestrial locomotion of a mole cricket with foreleg amputation. *Sci China Technol Sci* 58:999–1006.